DESIGN OF DUAL-BAND BANDPASS FILTERS WITH CONTROLLABLE BANDWIDTHS USING NEW MAPPING FUNCTION

G. Chaudhary[1], Y. Jeong[1, *], K. Kim[2], and D. Ahn[3]

[1]Division of Electronics and Information Engineering & IT Convergence Research Center, Chonbuk National University, 664-14, Deokjin-dong, Deokjin-gu, Jeonju 561-756, Republic of Korea

[2]Micro System Integration Center, Tohoku University, Sendai, Miyagi, Japan

[3]Department of Electrical Communication Engineering, Soonshunhyang University, Asan, Chungnam, Republic of Korea

Abstract—In this paper, a novel design method for a dual-band bandpass filter (BPF) with arbitrary controllable bandwidths based on a simple frequency mapping function is proposed and its analytical design equations are also derived. The circuit conversion techniques are employed for implementation with distributed transmission line. To validate the proposed dual-band BPF with controllable bandwidths, a low temperature co-fired ceramic (LTCC) transmission line as well as microstrip lines are used, respectively. The two types of design for the dual-band BPF have the same and significantly different fractional bandwidths (FBWs), respectively. The first type of dual-band BPF with same FBWs are implemented at 2.11–2.17 and 3.45–3.55 GHz. The second type of dual-band BPF with different FBWs are implemented at 3.40–3.60 and 5.15–5.25 GHz. The measured and theoretical results show good agreement, significantly validating the proposed frequency mapping function methodology.

1. INTRODUCTION

In modern wireless communication systems, the demand for multipurpose wireless applications is tending toward developments of multi-functional/band RF systems. In this trend, the development

of multi-functional/band components such as hybrids, power dividers, power amplifiers, antenna and microwave filters play an important role [1, 2].

Extensive researches on the design of dual-band BPFs have been presented [3–34]. One of simplest methods to design the dual-band BPF is by connecting two different passband BPFs in parallel to obtain the dual-band characteristics [3–7]. Another approach is to insert a narrowband bandstop filter into the broadband BPF to create the dual-band characteristics using Z-transform synthesis [8]. Because two different filters are used, the size of these dual-band BPF are comparatively large.

Another straightforward approach is to optimize both the physical dimensions and structures of dual-band BPF in order to meet the required dual-band BPF specifications using optimization techniques such as genetic algorithms [9]. These methods are based on a numerical optimization technique in the filter synthesis process, which requires a long optimization time.

In order to avoid the optimization technique, a method called the frequency transformation technique has been presented in designing the dual-band BPF.

Using a successive frequency transformation, a design of a dual-band BPF is presented in [10]. Although the central frequencies of dual-passbands can be chosen separately, the design process requires the same FBWs for the first and second passbands. A design of a dual-wideband passband BPF using the frequency mapping is presented in [11].

A lumped element dual-band BPF implemented with LTCC technology is presented in [12]. Although the size of the filter is compact, the out-of-band characteristics are worse. A design methodology for dual-band BPF using an artificial lumped-element coplanar waveguide (CPW) is presented in [13].

Currently, the coupling matrix method is widely used for designing dual-band or multi-band microwave filters. One method is to find a suitable coupling matrix such that the dual-band or multi-band response is created by placing the transmission zeros within the wideband BPF [14]. This method requires an initial estimation of the coupling coefficients because of the optimization process. In addition, the implementation requires sufficiently large coupling coefficients to meet the overall specifications of dual-band BPF.

Recently, multi-mode resonators such as stepped impedance resonators (SIRs), stub loaded SIRs, short/open stub loaded $\lambda/2$ wavelength dual-mode resonators, ring resonators, meander-loop resonators and complement split-ring resonator (CSRR) defected

ground structure, beeline compact microstrip resonator (BCMRC), composite right/left handed (CRLH) metamaterial resonators were widely used for designing dual-band BPFs by utilizing higher resonant modes of the resonator [15–32]. The resonant modes of the SIR can be controlled by the characteristic impedances of the high and low sections of the resonator. However, these approaches encounter difficulties when adjusting for the coupling coefficients between neighboring resonators in order to meet the dual-band specifications simultaneously. Additionally, in some cases, dual-band transformers are required to match the port impedance [33], which increases the implementation area. In [34], dual-band BPF with controllable bandwidths has been presented. However, these require some complex and time consuming mathematical calculation to find the desired element values of filter.

This paper presents a novel frequency mapping function to design a dual-band BPF with controllable bandwidths. The major benefit of the proposed frequency mapping function is that the individual frequency bandwidths can be controlled separately. In order to implement the design with distributed transmission lines, circuit conversion techniques have been employed. This paper is organized as follows. Section 2 describes the design procedure for the dual-band BPF using the new frequency mapping function. The design examples are demonstrated in Sections 3 and 4 followed by the simulation and experimental results. Section 5 concludes the paper.

2. DESIGN THEORY

Figure 1 shows the n-poles prototype low pass filters (LPFs). The element values of LPF can be obtained using the well known formula given in [35]. Fig. 2 shows typical Chebyshev LPF attenuation characteristics. In this case, L_{Ar} is the maximum insertion loss in the passband, while ω_1' is equal-ripple passband edge frequency.

Figure 3 shows the circuit diagrams of the proposed dual-band BPF and its attenuation characteristics. The frequency response characteristics of the proposed dual-band BPF can be obtained by mapping the frequency response of LPF. The frequency $-\omega_1'$ of LPF is mapped to ω_1 and ω_3 and the frequency ω_1' is mapped to ω_2 and ω_4, respectively, where ω_1 and ω_2 are the lower and the upper edge angular frequencies of the first passband and ω_3 and ω_4 are the lower and the upper edge angular frequencies of the second passband, as shown in Fig. 3(c).

The series-branch circuit elements of the proposed dual-band BPF can be obtained from the series circuit elements of LPF. The input
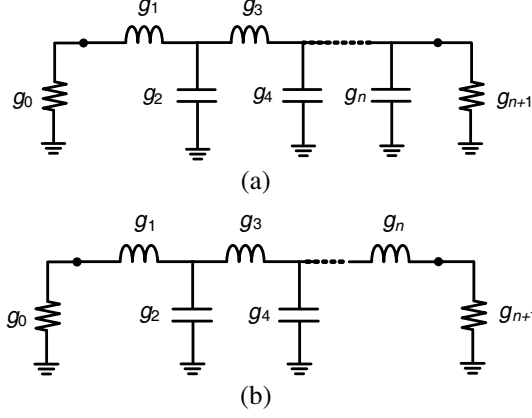
Figure 1. Prototype low-pass filter elements: (a) n is even and (b) n is odd.
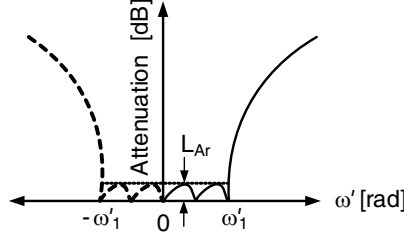
Figure 2. Chebyshev low-pass filter characteristic.

impedance of the series elements of LPF is given as:

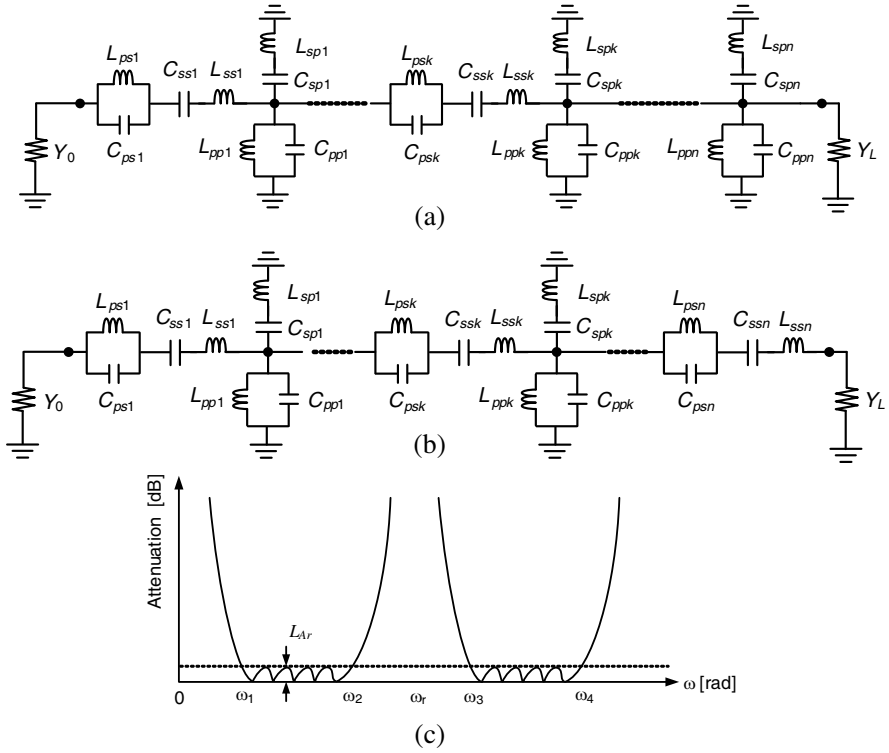$$Z'_{\text{in\_series}} = j\omega' g_k = jX'_{\text{series}} \tag{1}$$

Similarly, considering the series-branch elements of the proposed dual-band BPF, the input impedance is given as:

$$Z_{\text{in\_series}} = j\left(\frac{\omega L_{psk}}{1 - \frac{\omega^2}{\omega_{ops}^2}} - \frac{1 - \frac{\omega^2}{\omega_{oss}^2}}{\omega C_{ssk}}\right) = jX_{\text{series}} \tag{2}$$

The values of ω_{ops} and ω_{oss} are given as:

$$\omega_{ops} = \frac{1}{\sqrt{L_{psk}C_{psk}}} \tag{3}$$

$$\omega_{oss} = \frac{1}{\sqrt{L_{ssk}C_{ssk}}} \tag{4}$$

Figure 3. The circuit elements of the proposed dual-band BPF: (a) n is even, (b) n is odd, and (c) Chebyshev dual-band BPF attenuation characteristics.

Figure 4 shows the reactance characteristics of the series-branch of the LPF and the proposed dual-band BPF. From the reactance characteristics shown in Fig. 4, it can be inferred that the sum of the reactance at ω_1, ω_2 and at ω_3, ω_4 is zero, respectively. Similarly, the reactance at ω_1 is equal to the reactance at ω_3 and the reactance at ω_2 is equal to the reactance at ω_4, as indicated in (5)–(8).

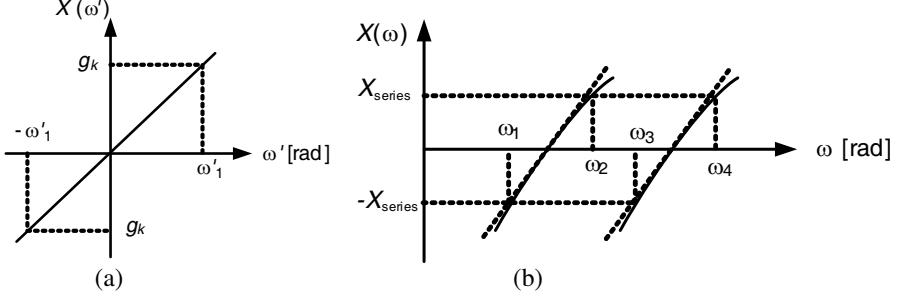$$X_{\text{series}}(\omega_1) + X_{\text{series}}(\omega_2) = 0 \qquad (5)$$

$$X_{\text{series}}(\omega_3) + X_{\text{series}}(\omega_4) = 0 \qquad (6)$$

$$X_{\text{series}}(\omega_1) = X_{\text{series}}(\omega_3) \qquad (7)$$

$$X_{\text{series}}(\omega_2) = X_{\text{series}}(\omega_4) \qquad (8)$$

From (2) and (5)–(8), the mapping function is given as:

$$L_{psk}C_{ssk} = \frac{A_1 + A_2}{B_1 + B_2} = \frac{A_3 + A_4}{B_3 + B_4} = \frac{A_1 - A_3}{B_1 - B_3} = \frac{A_2 - A_4}{B_2 - B_4} = \alpha \qquad (9)$$

Figure 4. The reactance characteristics of the series branch: (a) low-pass filter and (b) dual-band BPF.

The value of A_i and B_i are given as:

$$A_i = \frac{1 - \frac{\omega_i^2}{\omega_{oss}^2}}{\omega_i} \tag{10}$$

$$B_i = \frac{\omega_i}{1 - \frac{\omega_i^2}{\omega_{ops}^2}} \ , \ i = 1, 2, 3, 4 \tag{11}$$

Using (1), (2), and (9) for $\omega' = \omega_1' = 1$ and $\omega = \omega_2$, the series-branch circuit element values of the proposed dual-band BPF can be obtained as:

$$L_{psk} = \frac{g_k Z_0}{\left(\frac{\omega_2}{1 - \frac{\omega_2^2}{\omega_{ops}^2}} - \frac{1 - \frac{\omega_2^2}{\omega_{oss}}}{\omega_2 \alpha} \right)} \tag{12}$$

$$C_{psk} = \frac{1}{\omega_{ops}^2 L_{psk}} \tag{13}$$

$$C_{ssk} = \frac{\alpha}{L_{psk}} \tag{14}$$

$$L_{ssk} = \frac{1}{\omega_{oss}^2 C_{ssk}}, \ k = 1, 2, \dots n \tag{15}$$

Here, Z_0 is the termination impedance.

Similarly, the shunt-branch circuit elements of the proposed dual-band BPF can be obtained from the shunt-branch circuit elements of LPF. The input admittance of the shunt-branch elements of LPF is given as:

$$Y'_{\text{in\_shunt}} = j\omega' g_k = jB'_{\text{shunt}} \tag{16}$$

The input admittance of the shunt-branch elements of the proposed dual-band BPF is given as:

$$Y_{\text{in\_shunt}} = j \left(\frac{\omega C_{spk}}{1 - \frac{\omega^2}{\omega_{osp}^2}} - \frac{1 - \frac{\omega^2}{\omega_{opp}^2}}{\omega L_{ppk}} \right) = j B_{\text{shunt}} \qquad (17)$$

The values of ω_{osp} and ω_{opp} are given as:

$$\omega_{osp} = \frac{1}{\sqrt{L_{spk} C_{spk}}} \qquad (18)$$

$$\omega_{opp} = \frac{1}{\sqrt{L_{ppk} C_{ppk}}} \qquad (19)$$

Figure 5 shows the susceptance characteristics of the shunt-branch of the LPF and the proposed dual-band BPF. Similar to the series element case, from the susceptance graph of the dual-band BPF, the susceptance equations can be written as:

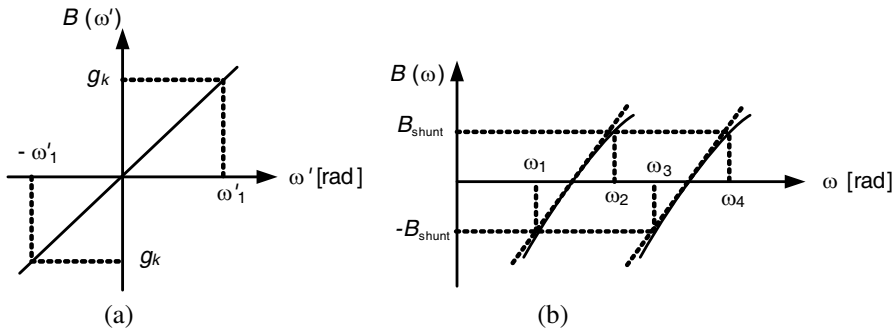$$B_{\text{shunt}}(\omega_1) + B_{\text{shunt}}(\omega_1) = 0 \qquad (20)$$

$$B_{\text{shunt}}(\omega_3) + B_{\text{shunt}}(\omega_4) = 0 \qquad (21)$$

$$B_{\text{shunt}}(\omega_1) = B_{\text{shunt}}(\omega_3) \qquad (22)$$

$$B_{\text{shunt}}(\omega_2) = B_{\text{shunt}}(\omega_4) \qquad (23)$$

Using (17) and (20)–(23), the mapping function is given as:

$$L_{ppk} C_{ppk} = \frac{C_1 + C_2}{D_1 + D_2} = \frac{C_3 + C_4}{D_3 + D_4} = \frac{C_1 - C_3}{D_1 - D_3} = \frac{C_2 - C_4}{D_2 - D_4} = \beta \quad (24)$$

Figure 5. Susceptance characteristics of shunt branch: (a) low-pass filter and (b) dual-band BPF.

The values of C_i and D_i are given as:

$$C_i = \frac{1 - \frac{\omega_i^2}{\omega_{opp}^2}}{\omega_i} \tag{25}$$

$$D_i = \frac{\omega_i}{1 - \frac{\omega_i^2}{\omega_{osp}^2}} \;,\; i = 1, 2, 3, 4 \tag{26}$$

The values of ω_{opp} and ω_{osp} have already been given by (18) and (19), respectively. Using (16), (17) and (24) for $\omega' = \omega_1' = 1$ and $\omega = \omega_2$, the shunt-branch circuit element values of the proposed dual-band BPF can be obtained as:

$$C_{spk} = \frac{g_k}{\left(\frac{\omega_2}{1 - \frac{\omega_2^2}{\omega_{osp}^2}} - \frac{1 - \frac{\omega_2^2}{\omega_{opp}^2}}{\omega\beta} \right) Z_0} \tag{27}$$

$$L_{spk} = \frac{1}{\omega_{osp}^2 C_{spk}} \tag{28}$$

$$L_{ppk} = \frac{\beta}{C_{spk}} \tag{29}$$

$$C_{ppk} = \frac{1}{\omega_{osp}^2 L_{ppk}}, \;\; k = 1, 2, \ldots n \tag{30}$$

The circuit of the proposed dual-band BPF shown in Fig. 3 consists of both series and parallel LC resonators circuits in the series and shunt-branches. These circuits are difficult to implement using only lumped elements at the microwave frequencies. In order to implement the above circuits of the proposed BPF with a planar transmission line, the circuit conversion technique is employed. By applying the circuit conversion technique, the series-branch elements are replaced with admittance inverters (J-inverters), which are shown in Fig. 6(a). For odd values of i, the circuit elements of Fig. 6(a) are given by (31)–(34).

$$C_{a1} = J_{01}^2 L_{ss1} \;,\; L_{a1} = \frac{C_{ss1}}{J_{01}^2} \tag{31}$$

$$L_{b1} = \frac{C_{ps1}}{J_{01}^2} \;,\; C_{b1} = J_{01}^2 L_{ps1} \tag{32}$$

$$C_{ai} = \frac{J_{01}^2 \ldots J_{l+2,l+3}^2}{J_{12}^2 \ldots J_{m+2,m+3}^2} L_{ssi} \;,\; L_{ai} = \frac{J_{12}^2 \ldots J_{m+2,m+3}^2}{J_{01}^2 \ldots J_{l+2,l+3}^2} C_{ssi} \tag{33}$$

$$L_{bi} = \frac{J_{12}^2 \ldots J_{m+2,m+3}^2}{J_{01}^2 \ldots J_{l+2,l+3}^2} C_{psi} \;,\; C_{bi} = \frac{J_{01}^2 \ldots J_{l+2,l+3}^2}{J_{12}^2 \ldots J_{m+2,m+3}^2} L_{psi} \tag{34}$$

The values of l and m are given as (35).

$$l = 0, 1, \ldots, \frac{i-3}{2}, \ m = 1, 2, \ldots \frac{i-3}{2} @ \ i = 1, 3, \ldots, n \qquad (35)$$

When the value of i is even, the circuit elements of Fig. 6(a) are given by (36)–(37).

$$C_{ai} = \frac{J_{12}^2 \ldots J_{l+2,l+3}^2}{J_{01}^2 \ldots J_{l+1,l+2}^2} C_{ppi}, \ L_{ai} = \frac{J_{01}^2 \ldots J_{l+1,l+2}^2}{J_{12}^2 \ldots J_{l+2,l+3}^2} L_{ppi} \qquad (36)$$

$$C_{bi} = \frac{J_{12}^2 \ldots J_{l+2,l+3}^2}{J_{01}^2 \ldots J_{l+1,l+2}^2} L_{spi}, \ L_{bi} = \frac{J_{01}^2 \ldots J_{l+1,l+2}^2}{J_{12}^2 \ldots J_{l+2,l+3}^2} L_{spi} \qquad (37)$$

The value of l in this case is given as (38)

$$l = 1, 2, \ldots, \frac{i-2}{2} @ \ i = 2, 4, \ldots, n \qquad (38)$$

The circuit shown in Fig. 6(a) consists of both the series and parallel LC resonators in the shunt-branch. The parallel LC resonator can be replaced with the series LC resonator by utilizing the J-inverter and the circuit conversation technique. The modified circuit, which consists of only the series LC resonators and J-inverters, are shown in Fig. 6(b). The circuit elements shown in Fig. 6(b) are given as:

$$J_{xi} = \sqrt{\frac{C_{ai}}{L_{x_i}}} = \sqrt{\frac{C_{xi}}{L_{a_i}}} \ i = 1, 2, \ldots, n \qquad (39)$$

Theoretically, the chosen J-inverter values can be arbitrary, however, in practice, J-inverter values should be chosen such that its physical dimensions can be realized without any difficulties. Introducing flexibility in the choice of J-inverter values allow the designer more freedom in the design and realization of the proposed dual-band BPFs.

3. LTCC FILTER IMPLEMENTATION

In order to validate the proposed structure shown in Fig. 6(a) obtained from the novel frequency mapping function, two types of filters have been designed, simulated and measured with LTCC technology. The BPFs have been fabricated on a substrate of RN2 with a dielectric constant of 7.8 and a loss tangent of 0.003. The J-inverters are implemented with a quarter-wavelength transmission line [35] at the frequency $f_{or} = (f_{01} f_{02})^{0.5}$, where $f_{01} = (f_1 f_2)^{0.5}$ is the geometric mean

of the first passband edge frequencies (f_1, f_2) and $f_{02} = (f_3 f_4)^{0.5}$ is
the geometric mean of the second passband edge frequencies (f_3, f_4).
Similarly, the series and parallel LC resonators in the shunt-branch

(a)

(b)
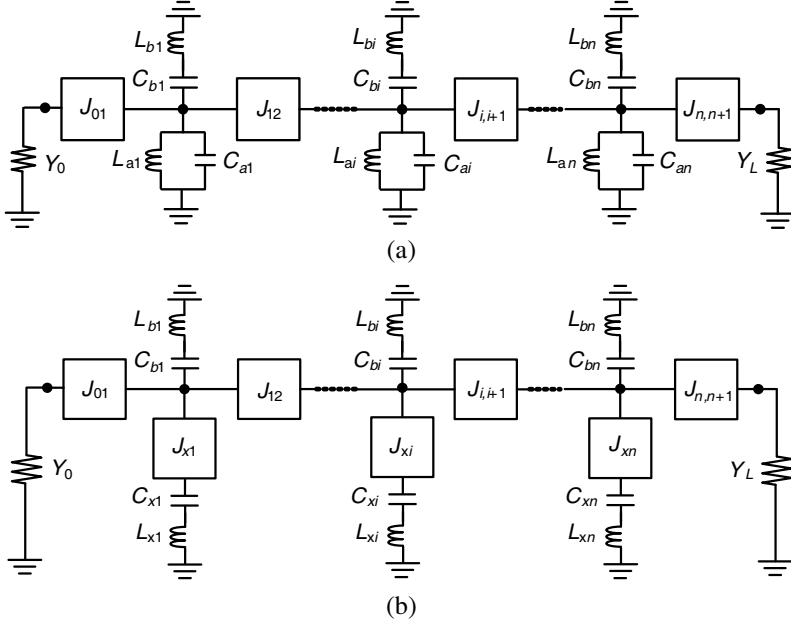
Figure 6. Circuit of proposed dual-band BPF with (a) J-inverters,
series and shunt LC resonators, and (b) J-inverters and only series LC
resonators.

(a)   (b)
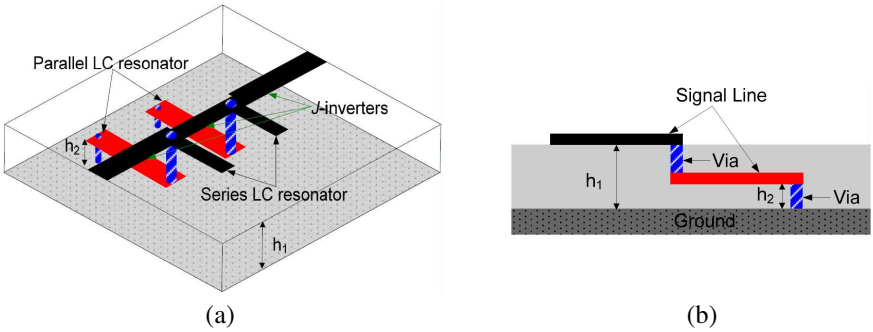
Figure 7. Fabricated LTCC dual-band BPF: (a) 3-D structure and
(b) side-view ($h_1 = 1.3$, $h_2 = 0.2$, [mm]).

are also implemented with the open-stub and short-stub quarter-wavelength transmission line with characteristic impedances Z_o and Z_s, at f_{oss} and f_{osp}, respectively. The 3-D structure and associated side-view of the fabricated LTCC BPF are shown in Fig. 7. The simulation utilized the Advanced Design System (ADS) 2009 of Agilent and the full-wave electromagnetic (EM) simulator HFSS v11 of Ansoft.

3.1. Dual-band Filter with Same Fractional Bandwidths

The Filter I specification utilizes almost the same FBWs. The frequencies are specified as: $f_1 = 2.11\,\text{GHz}$, $f_2 = 2.17\,\text{GHz}$, $f_3 = 3.45\,\text{GHz}$ and $f_4 = 3.55\,\text{GHz}$, where the FBW of the first and second passband are $\Delta_1 = 2.80\%$ and $\Delta_2 = 2.85\%$, respectively. The calculated values of f_{oss} (or f_{opp}) and f_{ops} (or f_{osp}) are 2.7427 GHz and 2.7303 GHz, respectively. The prototype elements of the second-order Chebyshev filter with the passband ripple of 0.01 dB are as: $g_0 = 1$, $g_1 = 0.4488$, $g_2 = 0.4077$ and $g_3 = 1.1007$.
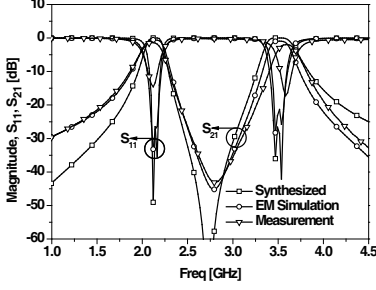
The calculated element values of the circuit shown in Fig. 6(a) are given as: $J_{01} = J_{23} = 0.0147$, $J_{12} = 0.0113$, $C_{a1} = C_{a2} = 4.8276\,\text{pF}$, $L_{a1} = L_{a2} = 0.6975\,\text{nH}$, $C_{b1} = C_{b2} = 1.1935\,\text{pF}$, $L_{b1} = L_{b2} = 2.8471\,\text{nH}$, $Z_s = 9.44\,\Omega$ and $Z_o = 62.18\,\Omega$.

The short stub resonators have relatively too low characteristic impedances, making them difficult to implement in microstrip lines. This is because low impedance requires a very large width that is even larger than the length of transmission line. The solution to this issue involves utilization of LTCC technology, where the low and the high impedance transmission lines can be implemented within a practical width range, by controlling the height (h_2 and h_1) of the substrate layers.

Figure 8 shows comparison results of the synthesized response, simulation and measurement for Filter I. There is good agreement between the synthesized response, simulation and measurement results except for a slight frequency shift in the measurement due to via misalignment during the LTCC manufacturing process. The measured insertion losses are 1.31 dB and 1.92 dB at frequencies of 2.12 GHz and 3.59 GHz, respectively. Similarly, the measured return losses are 15.3 dB and 17.98 dB at these frequencies. The bandwidths at the first and second passbands are 66.8 MHz and 96.8 MHz, for which the FBWs are 3.16% and 2.70%, respectively.

3.2. Dual-band Filter with Different Fractional Bandwidths

The specifications for Filter II utilize different FBWs. The frequencies are specified as: $f_1 = 3.4\,\text{GHz}$, $f_2 = 3.6\,\text{GHz}$, $f_3 = 5.15\,\text{GHz}$ and

Figure 8. Synthesized, simulated and measurement results of fabricated LTCC Filter I.
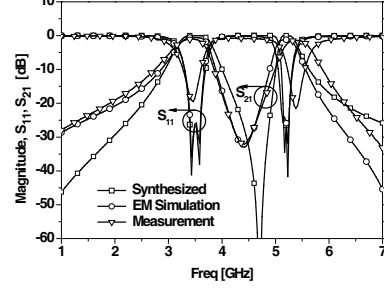
Figure 9. Synthesized, simulated and measurement results of fabricated LTCC Filter II.

$f_4 = 5.25$ GHz, for which the FBW of the first and second passband are $\Delta_1 = 5.71\%$ and $\Delta_2 = 1.92\%$, respectively. The prototype elements of a second-order Chebyshev LPF with the passband ripple of 0.01 dB are the same as Filter I. The calculated values of f_{oss} (or f_{opp}) and f_{ops} (or f_{osp}) are 3.8693 GHz and 4.7016 GHz, respectively. The calculated element values of the circuit shown in Fig. 6(a) are given as: $J_{01} = J_{23} = 0.0185$, $J_{12} = 0.0179$, $C_{a1} = C_{a2} = 4.0825$ pF, $L_{a1} = L_{a2} = 0.4144$ nH, $C_{b1} = C_{b2} = 0.4029$ pF, $L_{b1} = L_{b2} = 2.8442$ nH, $Z_s = 7.91 \, \Omega$, and $Z_o = 106.98 \, \Omega$.

Figure 9 shows the synthesized response, the simulation and measurement results of Filter II. The measured insertion losses are 1.01 dB and 1.39 dB at the frequencies of 3.47 GHz and 5.36 GHz, respectively. Similarly, the measured return losses are 18.35 dB and 21.79 dB at these frequencies. The bandwidths at the first and second passbands are 192.1 MHz and 96.8 MHz, respectively, for which the FBWs are 5.53% and 1.81%, respectively.

4. MICROSTRIP LINES FILTER IMPLEMENTATION

In order to validate the proposed structure shown in Fig. 6(b) obtained from the novel frequency mapping function, another two types of BPFs with microstrip lines have been designed, simulated and measured. The filters are fabricated on the Rogers RT/duroid 5880 substrate with a dielectric constant (ε_r) of 2.2 and a thickness (h) of 31 mils.

4.1. Dual-band Filter with Same Fractional Bandwidths

The specification of the Filter III is the same as for Filter I in the previous section. The calculated values of elements shown in Fig. 6(b)
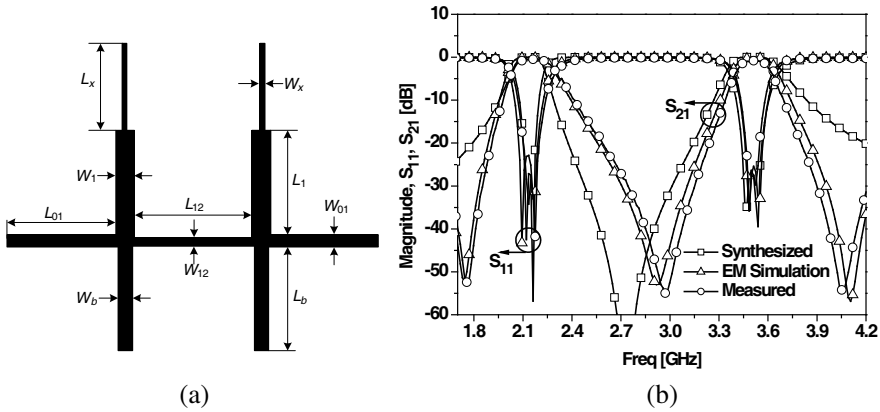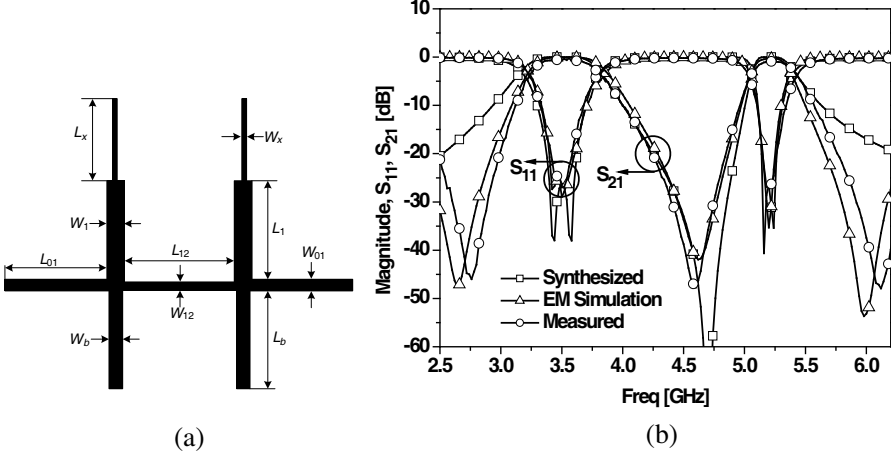
Figure 10. Proposed microstrip dual-band Filter III (a) physical layout, and (b) synthesized, simulation and measurement results.

for $n = 2$ are $J_{01} = J_{23} = 0.018$, $J_{12} = 0.0174$, $J_1 = J_2 = 0.037$, $L_{b1} = L_{b2} = 1.8590\,\text{nH}$, $C_{b1} = C_{b2} = 1.8290\,\text{pF}$, $L_{x1} = L_{x2} = 5.4012\,\text{nH}$, $C_{x1} = C_{x2} = 0.6234\,\text{pF}$. The physical layout and dimensions of Filter III shown in Fig. 10(a) are $W_{01} = 2.4$, $L_{01} = 19$, $W_{12} = 2.1$, $L_{12} = 18.2$, $W_x = 1$, $L_x = 19.5$, $W_1 = 2.9$, $L_1 = 18$, $W_b = 2.2$, $L_b = 18.4\,\text{mm}$, respectively.

Figure 10(b) shows synthesized response, the simulation and measurement results of Filter III. The measurement and simulation results are in good agreement. The measured in-band insertion losses are $0.6\,\text{dB}$ and $0.96\,\text{dB}$ at $2.14\,\text{GHz}$ and $3.5\,\text{GHz}$, respectively. The return loss at 2.11–$2.17\,\text{GHz}$ and 3.45–$3.55\,\text{GHz}$ in the first and second passband respectively, is greater than $21\,\text{dB}$. The measured bandwidths at the first and second passbands are 68.7 and $93.7\,\text{MHz}$, respectively, for which the FBWs are 3.21% and 2.68%, respectively. The attenuation is greater than $20\,\text{dB}$ at frequencies of 2.6–$3.25\,\text{GHz}$ between the two passbands, which provides a good level of isolation between them.

4.2. Dual-band Filter with Different Fractional Bandwidths

The Filter IV specification is the same as for Filter II in the previous section. The calculated values of elements shown in Fig. 6(b) for $n = 2$ are $J_{01} = J_{23} = 0.0172$, $J_{12} = 0.0155$, $J_1 = J_2 = 0.032$, $L_{b1} = L_{b2} = 3.2970\,\text{nH}$, $C_{b1} = C_{b2} = 0.3476\,\text{pF}$, $L_{x1} = L_{x2} = 3.4393\,\text{nH}$, $C_{x1} = C_{x2} = 0.4919\,\text{pF}$. The physical layout of Filter IV is shown in Fig. 11(a) and the dimensions are $W_{01} = 2.178$, $L_{01} = 11.90$,

(a)   (b)

Figure 11. Proposed microstrip dual-band Filter IV: (a) physical layout, and (b) synthesized simulation & measurement results.

$W_{12} = 1.60$, $L_{12} = 11.96$, $W_x = 0.4$, $L_x = 12$, $W_1 = 2.2$, $L_1 = 12.10$, $W_b = 0.596$, and $L_b = 11.86$ mm, respectively.

Figure 11(b) shows comparison results of the synthesized response, simulation and measurement of filter IV. The measured insertion losses in the passbands are 0.65 dB and 1.01 dB at 3.5 GHz and 5.2 GHz, respectively. The return loss at 3.4–3.6 GHz and 5.15–5.25 GHz are greater than 19 dB. The measured bandwidths are 190.6 MHz and 101.2 MHz, for which the FBWs are 5.44% and 1.94%, respectively.

5. CONCLUSION

We demonstrated a design method for a dual-band bandpass filter with arbitrary controllable bandwidths. A novel frequency mapping function was used in this paper. Simple analytical design equations are presented and the circuit elements of the proposed dual-band bandpass filters are calculated from the low-pass filter by applying a simple frequency mapping function. In order to implement the dual-band bandpass filter for the microwave frequency, circuit conversion techniques have been applied for easy realization with distributed transmission lines.

In order to validate the proposed method, two filters having the same and different fractional bandwidths are presented with LTCC as well as microstrip-line technology. The simulation and measurements results are in good agreement with the theoretical design results. The

proposed method is flexible enough to enable the design of bandpass filters with two passbands of significantly different bandwidths.

REFERENCES

1. Wu, Y. L., Y. A. Liu, S. L. Li, C. P. Yu, and X. Liu, "Closed form design method of an N-way dual-band Wilkinson hybrid power divider," *Progress In Electromagnetics Research*, Vol. 101, 97–114, 2010.

2. Li, B., X. Wu, N. Yang, and W. Wu, "Dual-band equal/unequal Wilkinson power dividers based on coupled-line section with short-circuited stub," *Progress In Electromagnetics Research*, Vol. 111, 163-178, 2011.

3. Abu-Hundrouss, A. M. and M. J. Lancaster, "Design of multiple-band microwave filters using cascaded filter elements," *Journal of Electromagnetic Waves and Applications*, Vol. 23, No. 16, 2109–2118, 2009.

4. Hung, C. Y., R. Y. Yang, and Y. L. Lin, "A simple method to design a compact and high performance dual-band bandpass filter for GSM and WLAN," *Progress In Electromagnetics Research C*, Vol. 13, 187–193, 2010.

5. Lai, X., N. Wang, B. Wu, and C. H. Liang, "Design of dual-band filter based on OLRR and DSIR," *Journal of Electromagnetic Waves and Applications*, Vol. 24, No. 2/3, 209–218, 2010.

6. Yang, R. Y., K. Hon, C. Y. Hung and C. S. Ye, "Design of dual-band bandpass filters using a dual feeding structure and embedded uniform impedance resonators," *Progress In Electromagnetics Research*, Vol. 105, 93–102, 2010.

7. Liang, F., B. Luo, W. Lu, and X. Wang, "A compact dual-band filter with close passbands using asymmetric $\lambda/4$ resonator pairs with shared via-hole ground," *Journal of Electromagnetic Waves and Applications*, Vol. 25, No. 8/9, 1289-1296, 2011.

8. Tsai, L. C. and C. W. Hsue, "Dual-band bandpass filters using equal-length coupled serial-shunted lines and Z-transform technique," *IEEE Trans. Microw. Theory Tech.*, Vol. 52, No. 4, 1111–1117, Apr. 2004.

9. Lai, M. I. and S. K. Jeng, "Compact microstrip dual-band bandpass filters design using genetic-algorithm techniques," *IEEE Trans. Microw. Theory Tech.*, Vol. 54, No. 1, 160–168, Jan. 2006.

10. Guan, X., Z. Ma, P. Chai, Y. Kobayashi, T. Anada, and G. Hagiwara, "Synthesis of dual-band bandpass filters using successive frequency transformations and circuit conversions,"

IEEE Microw. Wireless Compon. Lett., Vol. 16, No. 3, 110–112, Mar. 2006.

11. Liu, A. S., T. Y. Huang, and R. B. Wu, "A dual wideband filter design using frequency mapping and stepped impedance resonators," *IEEE Trans. Microw. Theory Tech.*, Vol. 56, No. 12, 2921–2929, Dec. 2008.

12. Joshi, H. and W. J. Chappell, "Dual-band lumped element bandpass filter," *IEEE Trans. Microw. Theory Tech.*, Vol. 54, No. 12, 4169–4170, Dec. 2006.

13. Mao, S. G. and M. S. Wu, "Design of artificial lumped-element coplanar waveguide filters with controllable dual-passband responses," *IEEE Trans. Microw. Theory Tech.*, Vol. 56, No. 7, 1684–1692, Jul. 2008.

14. Mokhtaari, M., J. Bornemann, K. Rambabu, and S. Amari, "Coupling matrix design of dual and triple passband filters," *IEEE Trans. Microw. Theory Tech.*, Vol. 54, No. 11, 3940–3946, Nov. 2006.

15. Weng, M. H., C. H. Kao, and Y. C. Chang, "A compact dual-band bandpass filter with high band selectivity using cross-coupled asymmetric SIRs for WLANs," *Journal of Electromagnetic Waves and Applications*, Vol. 24, No. 2/3, 161–168, 2010.

16. Yang, R. Y., C. Y. Hung, and J. S. Lin, "A dual-band bandpass filter with an enhanced second passband performance using modifiable coupling," *Journal of Electromagnetic Waves and Applications*, Vol. 25, No. 2/3, 305–314, 2011.

17. Ma, D. C., Z. Y. Xiao, L. L. Xiang, X. H. Wu, C. Y. Huang, and X. Kou, "Compact dual-band bandpass filter using folded SIR with two stubs for WLAN," *Progress In Electromagnetics Research*, Vol. 117, 357–364, 2011.

18. Lee, C. H., I. C. Wang, and C. I. G. Hsu, "Dual-band balanced BPF using $\lambda/4$ stepped-impedance resonators and folded feed lines," *Journal of Electromagnetic Waves and Applications*, Vol. 23, No. 17/18, 2441–2449, 2009.

19. Alkanhal, M. A. S., "Dual-band bandpass filters using inverted stepped-impedance resonators," *Journal of Electromagnetic Waves and Applications*, Vol. 23, 1211–1220, 2009.

20. Chiou, Y. C., P. S. Yang, J. T. Kuo, and C. Y. Wu, "Transmission zero design graph for dual-mode dual-band filter with periodic stepped impedance ring resonator," *Progress In Electromagnetics Research*, Vol. 108, No. 8/9, 23–36, 2010.

21. Xiao, J. K. and H. F. Huang, "New dual-band bandpass filter with compact SIR structure," *Progress In Electromagnetics Research Letters*, Vol. 18, 125–134, 2010.

22. Sun, X. and E. L. Tan, "A novel dual-band bandpass filter using generalized trisection stepped impedance resonator with improved out-of-band performance," *Progress In Electromagnetics Research Letters*, Vol. 21, 31–40, 2011.

23. Wang, J. P., L. Wang, Y. X. Guo and Y. X. Wang, "Miniaturized dual-mode bandpass filter with controllable harmonic response for dual-band applications," *Journal of Electromagnetic Waves and Applications*, Vol. 23, No. 11/12, 1525–1533, 2009.

24. Velazquez-Ahumada, M. D. C., J. Martel, F. Medina, and F. Mesa, "Application of stub loaded folded stepped impedance resonators to dual band filter design," *Progress In Electromagnetics Research*, Vol. 102, 107–124, 2010.

25. Xu, K. D., Y. H. Zhang, C. L. Zhuge, and Y. Fan, "Miniaturized dual-band bandpass filter using short stub-loaded dual-mode resonators," *Journal of Electromagnetic Waves and Applications*, Vol. 25, No. 16, 2264–2273, 2011.

26. Chen, F. C. and J. M. Qiu, "Dual-band bandpass filter with controllable characteristics using stub-loaded resonators," *Progress In Electromagnetics Research Letters*, Vol. 28, 45–51, 2012.

27. Huang, C. Y., M. H. Weng, C. Y. Hung, and S. W. Lan, "Design of a dual-band bandpass filter for GSM and direct sequence ultra-wideband communication systems," *Journal of Electromagnetic Waves and Applications*, Vol. 25, No. 11/12, 1605–1615, 2011.

28. Kung, C. Y. and Y. C. Chen, "A novel compact 2.4/5.2 GHz dual wideband bandpass filter with deep transmission zero," *Journal of Electromagnetic Waves and Applications,* Vol. 25, No. 5/6, 617–628, 2011.

29. Ji, Y. X., J. Xu, Y. M. Niu, C. Z. Hua, C. H. Chen, and W. Wu, "Compact and high performance bandpass filter based on an improved hybrid resonator using beeline compact microstrip resonator cell (BCMRC)," *Journal of Electromagnetic Waves and Applications*, Vol. 25, No. 11/12, 1525–1535, 2011.

30. Chaudhary, G., Y. Jeong, and J. Lim, "A broad-bandwidth dual-band bandpass filter design using composite right/left handed transmission lines," *Journal of Electromagnetic Waves and Applications*, Vol. 25, No. 14/15, 2138–2147, 2011.

31. Wu, G. L., W. Mu, X. W. Dai, and Y. C. Jia, "Design of novel dual-band bandpass filter with microstrip meander-loop resonator

and CSRR DGS," *Progress In Electromagnetics Research*, Vol. 78, 17–24, 2008.

32. Wu, Y. L., C. Lia, and X. Z. Xiong, "A dual-wideband bandpass filter based on E-shaped microstrip SIR with improved upper-stoband performance," *Progress In Electromagnetics Research*, Vol. 108, 141–153, 2010.

33. Weng, M. H., H. W. Wu, and Y. K. Su, "Compact and low loss dual bandpass filter using pseudo-interdigital stepped impedance resonators for WLANs," *IEEE Microw. Wireless Compon. Lett.*, Vol. 17, No. 3, 187–189, Mar. 2007.

34. Guan, X., Z. Ma, P. Cai, T. anada, and G. Hagiwara, "Design of microstrip dual-band bandpass filter with controllable bandwidth," *Microw. Optical Tech. Letters*, Vol. 49, No. 3, 740–742, Mar. 2007.

35. Matthaei, G., L. Young, and E. M. T. Jones, *Microwave Filters, Impedance-matching Networks and Coupling Structures*, McGraw-Hill Book Co., New York, NY, 1964.